 doi:10.20944/preprints202011.0641.v1

Article

Monitoring Viral Entry in Real-Time Using a Luciferase Recombinant Vesicular Stomatitis Virus Producing SARS-CoV-2, EBOV, LASV, CHIKV, and VSV Glycoproteins

Maria Fernanda Lay-Mendoza [1], Marissa Danielle Acciani [1], Courtney Nina Levit [1], Christopher Santa Maria and Melinda Ann Brindley [2,*]

[1] Department of Infectious Diseases, College of Veterinary Medicine, University of Georgia, Athens, GA 30602, USA
[2] Department of Infectious Diseases, Department of Population Health, College of Veterinary Medicine, University of Georgia, Athens, GA 30602, USA
* Correspondence: mbrindle@uga.edu; Tel.: +1-706-542-5796

Abstract: Viral entry is the first stage in the virus replication cycle and, for enveloped viruses, is mediated by virally encoded glycoproteins. Viral glycoproteins have different receptor affinities and triggering mechanisms. We employed vesicular stomatitis virus (VSV), a BSL-2 enveloped virus that can incorporate non-native glycoproteins, to examine the entry efficiencies of diverse viral glycoproteins. To compare glycoprotein-mediated entry efficiencies of: VSV G, SARS-CoV-2 S, EBOV GP, LASV GP, and CHIKV E we produced recombinant VSV (rVSV) viruses that produce the five glycoproteins. The rVSV virions encoded a nano luciferase-PEST (NLucP) reporter gene, which we used in combination with the live-cell substrate Endurazine™ to monitor viral entry kinetics in real time. Our data indicate that rVSV particles with glycoproteins that require more post-internalization priming typically demonstrate delayed entry in comparison to VSV G. In addition to determining the time required for each virus to complete entry, we also used our system to evaluate viral cell surface receptor preferences, monitor fusion, and elucidate endocytosis mechanisms. This system can be rapidly employed to examine diverse viral glycoproteins and their entry requirements.

Keywords: entry; kinetics; luciferase; real-time; live assay, vesicular stomatitis virus; Ebola; Lassa; chikungunya; coronavirus.

1. Introduction

Enveloped viruses are covered in a lipid membrane acquired by budding from infected cells. In order for enveloped viruses to infect a cell, the viral membrane must fuse with the cellular membrane, creating a pore through which the viral genome enters the cell cytoplasm. To accomplish fusion, viruses produce fusion proteins studded in their membrane. To date, there are three defined classes of viral fusion proteins termed class I, II and III [1,2]. While all proteins from all three classes are capable of forming fusion pores between the viral and cellular membranes, they have different properties and requirements [1-3]. Here we produced a panel of recombinant vesicular stomatitis viruses (rVSV) containing five different viral fusion proteins, including representatives from each class. Experiments were designed to monitor entry kinetics and compare the efficiencies of the Lassa (LASV), Ebola (EBOV), severe acute respiratory syndrome coronavirus 2 (SARS-CoV-2), Chikungunya (CHIKV), and VSV glycoproteins.

Class I fusion proteins are translated as single polypeptides that fold into trimeric complexes. A cleavage event produces two subunits, which liberates the fusion peptide and converts the protein

Preprints (www.preprints.org) | NOT PEER-REVIEWED | Posted: 25 November 2020 doi:10.20944/preprints202011.0641.v1

into a fusion-ready state. While the pre-fusion structures and fusion triggers for class I proteins are variable, they all adopt a similar post-fusion six-helix bundle (6HB) conformation [1,2]. Coronavirus Spike (S) [4], LASV glycoprotein (GP), and EBOV GP are class I fusion proteins.

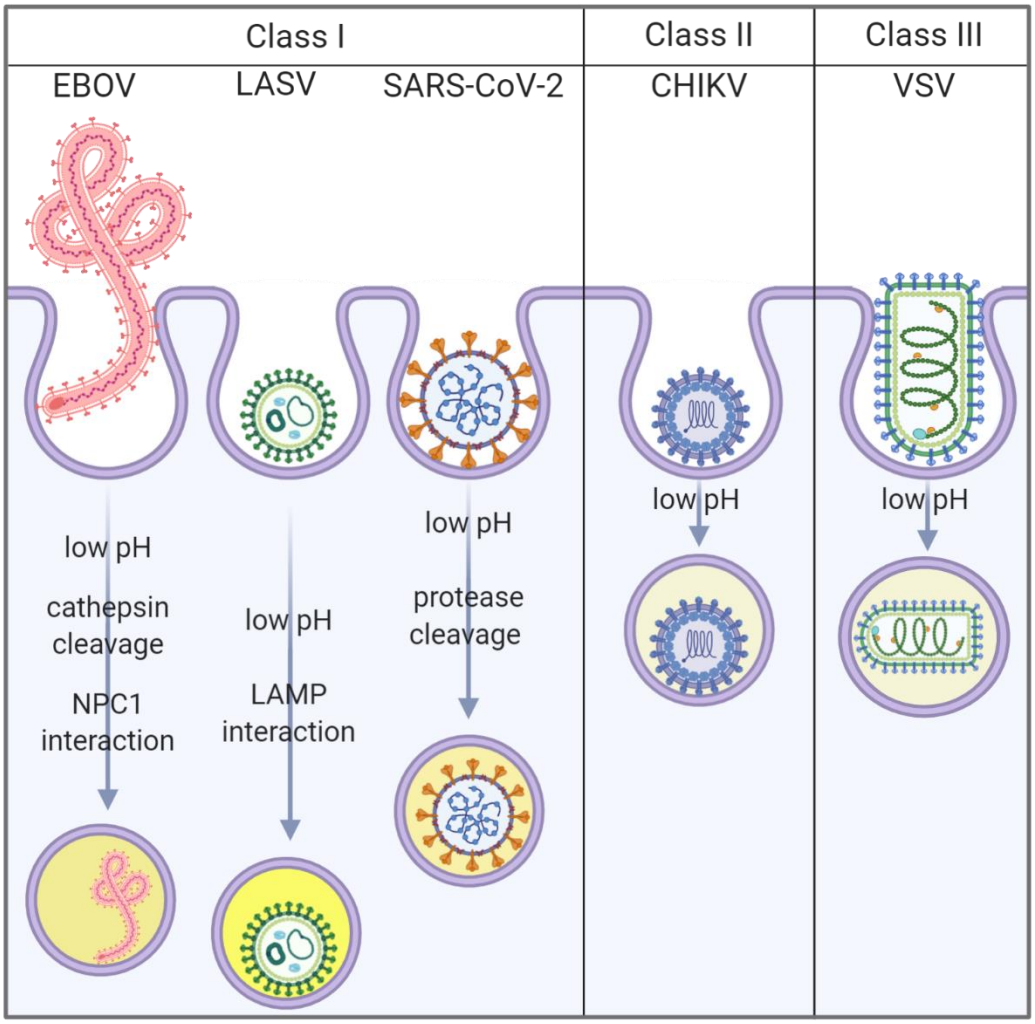

Figure 1. Schematic illustrating the entry pathways for viruses containing class I, class II, or class III fusion proteins, emphasizing the variety of conditions needed to prime the fusion proteins. CHIKV and VSV fusion occurs in early/less acidic endosomes (light yellow, close to the plasma membrane), while EBOV, LASV, and SARS-CoV-2 fusion occurs in late endosomes/endolysosomes (darker yellow, deeper in the cytoplasm). Created with BioRender.com

SARS-CoV-2 S initiates infection by interacting with cellular angiotensin-converting enzyme 2 (ACE2) [5,6]. Cellular proteases are required to expose the fusion peptide [7]. In cells with surface proteases, fusion can occur at the plasma membrane in a pH-independent manner [8]. Cells that lack surface proteases mediate entry through low pH activated cathepsins that cleave S in endosomes rather than the cell surface (Figure 1) [9,10]. S cleavage liberates the fusion peptide and triggers conformational changes that enable S to mediate membrane fusion, initiating infection.

Entry of LASV into cells primarily occurs through interaction with α-dystroglycan (αDG) on the cell surface [11,12]. Several attachment factors including heparan sulfate, C-type lectins, TIM-1, and Axl and Tyro3 from the TAM receptor family kinases [13-17] can mediate entry in the absence of functional αDG. Once the virion is within the endolysosomal compartment, low pH and Lysosomal Associated Membrane Protein 1 (LAMP1) induce a conformational change in the glycoprotein [15] resulting in fusion with the endosomal membrane [18]. While many fusion proteins are triggered by

Preprints (www.preprints.org) | NOT PEER-REVIEWED | Posted: 25 November 2020 doi:10.20944/preprints202011.0641.v1

low pH (pH<6), optimal LASV GP fusion activity requires highly acidic conditions (pH 4.5) (Figure 1) [19,20].

While there are no definitive cell surface receptors for EBOV, several types of cell surface proteins including lectins and phosphatidylserine (PtdSer) receptors have been described as important attachment factors to mediate internalization [21-24]. Once EBOV is in the endolysosomal compartment, low-pH activates cellular proteases that cleave GP [25], facilitating GP interaction with the endosomal receptor Niemann-Pick 1 (NPC1) which induces fusion with the endosomal membrane (Figure 1) [26].

Class II fusion proteins form dimeric pre-fusion complexes rich in β-sheets sitting parallel to the viral membrane [27]. Similar to class I proteins, class II fusion proteins form hair-pin structures during fusion which bring the membranes in close proximity [27]. The CHIKV E2/1 complex protein is a class II fusion protein; E2 is thought to be responsible for receptor-binding while E1 is essential for membrane fusion triggered by low pH in early endosomes (Figure 1) [28]. No receptors have been identified for CHIKV entry into all cells, but several attachment factors can facilitate virion internalization, including Mxra8 [29-33].

Class III fusion proteins form trimers in both the pre- and post-fusion (hairpin-like) conformations [34,35]. Rhabdovirus G proteins, herpesvirus gB [36], and baculovirus gp64 [37] are classified as class III fusion proteins. Unlike the class I and II fusion proteins that are metastable and irreversibly triggered, G folding is reversible and its conformation changes between pre- and post-fusion depending on the pH of the environment [38]. VSV is a prototypical rhabdovirus and its entry mechanism has been studied for decades [39,40]. VSV G mediates entry into an impressive number of cells through interaction with the low-density lipoprotein (LDL) receptor family [41,42], after which low pH in early endosomes triggers membrane fusion (Figure 1)[43].

The entry mechanisms of LASV, EBOV, and SARS-CoV-2 are relatively complex in comparison to those of CHIKV and VSV. SARS-CoV-2 and EBOV fusion require proteolytic glycoprotein processing, LASV and EBOV fusion requires endosomal receptor interactions, whereas CHIKV and VSV simply require exposure to low pH. To compare glycoprotein-mediated entry efficiencies, we infected a variety of commonly cultured cell lines with recombinant VSV (rVSV) expressing 5 different glycoproteins: native G, SARS-CoV-2 S, EBOV GP, LASV GP, or CHIKV E. While authentic EBOV, LASV, SARS-CoV-2, CHIKV, and VSV particles have different morphologies, all five glycoproteins are incorporated onto VSV. Our rVSV virions encoded a nano luciferase-PEST (NLucP) reporter gene, which we used in combination with live-cell substrate Endurazine™ to monitor viral entry kinetics in real time. Our data demonstrate both VSV G and CHIKV E can mediate rapid virus entry which is closely followed by SARS-CoV-2 S. Both LASV GP and EBOV GP entry were slower, but EBOV GP mediated entry occurred more rapidly if the GP was pre-treated with proteases. This system can be rapidly employed to examine diverse viral glycoproteins and their entry requirements.

2. Materials and Methods

2.1. Cell Lines and Transfections

Vero (vervet kidney cells) constitutively expressing human SLAM/CDw150 (signaling lymphocytic activation molecule 1) (referred to as VeroS) [44] and Baby Hamster's Kidney cells (BHK21) stably expressing T7 RNA polymerase [45] were maintained in high glucose Dulbecco's Modified Eagle Medium (DMEM) supplemented with 5% FBS (vol/vol). VeroS cells have a significantly higher transfection efficiency compared to VeroE6 and therefore are our preferred VeroS cell line for experiments. Human Embryonic Kidney cells (HEK293T) that expresses the SV40 large T antigen (kindly provided by Dr. Biao He from University of Georgia) were maintained in high glucose Dulbecco's Modified Eagle Medium (DMEM) supplemented with 10% FBS (vol/vol). Human haploid cells (HAP1) and HAP1 cells knocked-out for alpha dystroglycan (HΔDAG1) (Horizon Discovery, Cambridge, UK) were maintained in Iscove's media supplemented with 8% FBS [46]. All cells were kept at 37°C with 5% CO_2. BHK-T7 cell transfections were performed with GeneJuice

 doi:10.20944/preprints202011.0641.v1

(Millipore, Burlington, MA) and HEK293T cells were transfected with jetPRIME® (PolyPlus Transfection) according to the manufacturer's instructions.

2.2. Cloning and Rescue of Viruses

GFP from pVSVΔG/EBOV-GP-GFP and pVSVΔG/VSV-G-GFP molecular clones [47] was replaced with NlucP (Promega™, Madison, WI) utilizing NheI and AvrII restriction sites. To produce pVSV/LASV-GP-Nluc, the codon optimized protein coding region of Lassa Josiah strain [46] was amplified with additional MluI and NheI sites which were used to clone into the pVSVΔG_nLucP molecular clone. Similarly, Chikungunya (CHIKV) E protein (strain S27) [48] was amplified with additional MluI and NheI sites to produce pVSV/CHIKV-E-Nluc. pVSV/SARS-CoV-2-S was cloned by adding MluI and NheI sites to the codon optimized protein coding region of SARS-CoV-2 S from Wuhan strain. The S contains an additional 9 residues in the signal peptide [49] and the last 21 residues of the cytoplasmic tail were removed. In addition, D614G was introduced. Rescue of rVSV viruses was completed as previously described [47]. For experiments, the initial recovered virus was passaged onto a T75 of VeroS cells (P2 stocks) and in some instances the P2 stock was used to generate more virus (P3 stocks). Stocks and samples were titrated by serial diluting samples in media and determining the median tissue culture infectious dose ($TCID_{50}$) using the Spearman-Karber $TCID_{50}$ method [50]. For some experiments, stocks were titrated with plaque assay on VeroS cells as previously described [51].

CHIKV-Nluc was made by engineering the Nluc into the CHIKV-181/c25 genome as an additional transcription unit. Nluc was cloned in pSinRep5-181/25ic, a gift from[49] Terence Dermody (Addgene plasmid #60078) using overlapping PCR. To generate viral genomic RNA, the plasmid was linearized with NotI (NEB), *in vitro* transcribed and capped with the mMESSAGE mMACHINE SP6 Transcription Kit (Invitrogen). Viral RNA (1 μg) was transfected into VeroS cells with Lipofectamine 3000 (Invitrogen) and virus containing supernatants were collected when cells showed signs of cytopathic effect, approximately 48 following transfection. For experiments, the initial recovered virus was passaged onto a T75 of VeroS cells (P2 stocks).

2.3. Replication Curves of rVSV

VeroS cells were seeded in a 12-well plate at a density of $2x10^5$ cells/well. Cells were infected for 1 hour at 37°C with the indicated viruses at a MOI of 0.01 PFU/cell. Media was replaced and supernatants collected at time 0 (immediately) and the indicated time points, stored at -80°C, and titrated by serial diluting samples in media and determining the median tissue culture infectious dose ($TCID_{50}$) using the Spearman-Karber $TCID_{50}$ method [50].

2.4. Entry kinetics of rVSV into Vero cells

VeroS cells were seeded at a density of $2x10^4$ cells/well in a black-wall clear bottom 96-well plate. 48 hours post-seeding, Endurazine™ (Promega™, Madison, WI) was diluted 1:100 with DMEM and incubated with the cells for 1 hour at 37°C. Cells were infected at multiple MOIs (25, 5, 1, 0.2, 0.04) PFU/cell with virus in the presence of the substrate for an additional hour. In some experiments, cells were infected with the different viruses at an MOI 1 and ammonium chloride (NH_4Cl; 30 mM, pH 7.0) was added at various time points post infection to block subsequent fusion events. After the hour of infection, media was replaced with high-glucose phenol red-free DMEM (supplemented with 5% FBS and 25 mM HEPES). The plate was moved into a pre-warmed (37°C) plate reader, and luminescence was measured every 10 minutes at 37°C with a Glomax® Explorer (Promega™, Madison, WI).

2.5. rVSVΔG/LASVGP entry kinetics into HAP1 and HΔDAG1 cells

The day before infection, a 96-well plate black-wall clear bottom was seeded with $1.5x10^4$ cells/well. Entry inhibitors were pre-incubated with cells for 30 minutes at 37°C; then Endurazine (Promega, Madison, WI) was added to the cells at the time of infection. HAP1 were infected at a MOI

Preprints (www.preprints.org) | NOT PEER-REVIEWED | Posted: 25 November 2020 doi:10.20944/preprints202011.0641.v1

of 1 and HΔDAG1 cells were infected with 100 times more virus to reach similar infection rates. Luminescence was measured as described above. Entry inhibitors: EIPA (50 μM), dynasore (6.25 μM), nystatin (30 μg/ml), chlorpromazine hydrochloride (0.625 μg/ml) (all from Millipore Sigma, Burlington, MA), dissolved in either dimethyl sulfoxide (DMSO) or water.

2.6. Entry kinetics into HEK293T expressing attachment factors

HEK293T cells were seeded at a density of $3x10^4$ cells/well in a 96-well plate. 24 hours post-seeding, cells were transfected with either empty vector, pCS6-Axl (TransOMIC, Huntsville, AL [BC032229]), pCS6-Tyro3 (TransOMIC, Huntsville, AL [BC051756]), TIM-1-GFP [22], pCS6-L-SIGN (TransOMIC, Huntsville, AL, [BC038851]), or pcDNA-hACE2 (hACE2 was a gift from Hyeryun Choe (Addgene plasmid # 1786)) [52]. Two hours post-transfection, half of the media was replaced. 24-hour post-transfection, cells were infected at a MOI of 25 $TCID_{50}$ unit/cell for rVSVΔG/EBOV experiments and MOI 1 for rVSVΔG/SARS-CoV2 experiments in the presence of Endurazine™. Luminescence was measured every 10 minutes at 37°C in the presence of HEPES (25 mM).

2.7. Thermolysin cleavage of virus

rVSVΔG/VSV or rVSVΔG/EBOV were treated as described by the White lab [53]. Virus was incubated with thermolysin (Sigma P1512; 0.1 mg/ml in cleavage buffer (20 mM HEPES, pH 7.5, 20 mM morpholinepropanesulfonic acid, 130 mM NaCl) containing 2 mM $CaCl_2$ at 37°C for 1 h. The reaction was stopped with the addition of EDTA (10 mM). Viral particles were then purified from the thermolysin by loading onto an Amicon Ultra spin concentrator (300-kDa cutoff; Millipore) and washing the samples with 5 column volumes of cleavage buffer. Mock treated samples were processed in the same manner without adding thermolysin. Samples were titrated and no significant differences in infectivity was noted between mock and thermolysin cleaved samples. Cleavage was monitored by sodium dodecyl sulfate-polyacrylamide gel electrophoresis (SDS-PAGE) followed by immunoblot analysis of the viral glycoprotein.

2.8. Immunoblots

To detect attachment factors transfected into HEK293T cells, cells were pelleted (800 x g, 5 minutes), resuspended in 100 μl of 1X PBS, lysed with 100 μl M2 lysis buffer (50 mM Tris, pH 7.4, 150 mM NaCl, 1 mM EDTA, 1% Triton X-100), and cleared of insoluble material (17,000 x g, 30 min, 4°C). Samples were denatured in SDS-UREA buffer (200 mM Tris, pH 6.8, 8 M urea, 5% sodium dodecyl sulfate (SDS), 0.1 mM EDTA, 0.03% bromophenol blue, 1.5% dithiothreitol) for 30 minutes at 56°C, separated on a 4-20% Tris-Glycine SDS-PAGE gel (Invitrogen, Waltham, MA) and transferred to PVDF (Polyvinylidene difluoride) membranes. Membranes were incubated with antibodies against GAPDH (Santa Cruz Biotechnology, Dallas, TX [SC-47724, 1:2,000]), Axl (R&D Systems Minneapolis, MN, [AF154, 1:2,000]), GFP (Thermo Fisher, Waltham, MA, [A-6455, 1:1,000]), Tyro3 (R&D Systems Minneapolis, MN, [AF859, 1:1,000)], and L-SIGN (Thermo Fisher, Waltham, MA, [MA5-21012, 1:200]). Corresponding secondary antibodies conjugated with HRP were used to detect the proteins. Protein signals were detected with West Dura (ThermoFisher, Waltham, MA) and imaged on a BioRad ChemiDocXRS (Bio-Rad, Hercules, CA).

To detect viral envelope in thermolysin-treated and non-treated viral stocks, membranes were incubated with antibodies against EBOV GP (IBT Bioservices, Rockville, MD [0365-001]), VSV G (KeraFast, Boston, MA [EB0010]), and VSV M (KeraFast, Boston, MA[EB0011]).

3. Results

3.1. Recovery and replication rates of the rVSV viruses

Preprints (www.preprints.org) | NOT PEER-REVIEWED | Posted: 25 November 2020 doi:10.20944/preprints202011.0641.v1

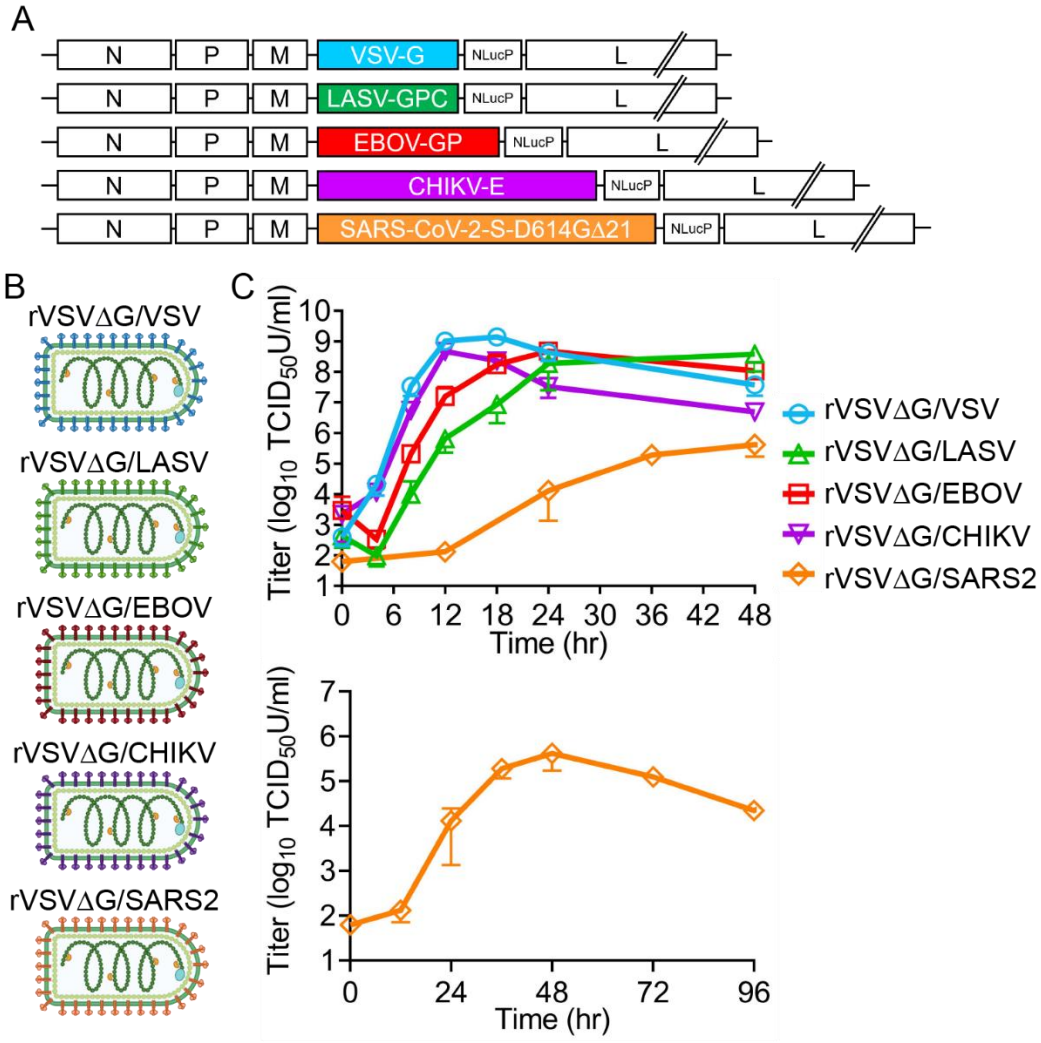

Figure 2. rVSVΔG chimeric viruses' replication curves. (**A**) Schematic representation of EBOV, LASV, SARS-CoV-2, CHIKV, and VSV envelope and NlucP reporter gene cloned into the molecular clone of VSV. (**B**) Viruses produced from the VSV molecular clones expressing different glycoproteins. Created with BioRender.com (**C**) Multi-cycle replication curves of the viruses on VeroS (MOI 0.01). Lower panel is the complete time course for rVSVΔG/SARS. Each experiment was repeated three independent times. Data shown are the averages and SEM.

To compare the entry efficiencies of EBOV, LASV, SARS2, CHIKV, and VSV, we cloned the glycoproteins into the molecular clone of VSV and inserted a reporter gene in a post-envelope location (Figure 2A). Viruses were recovered (Figure 2B) and all subsequent experiments were completed with pass 2 or 3 stocks amplified on VeroS cells. To monitor virus production over time, we performed multi-cycle replication curves, infecting cells at an MOI 0.01 (Figure 2C). VSV G and CHIKV E produced the highest titers of virus, and peak titers were observed sooner than the other rVSV viruses at 12 hours following infection. EBOV GP reached peak titers 24 hours following infection, and LASV required 48 hours. rVSVΔG/SARS2 replication was severly reduced compared to the other glycoproteins. While rVSVΔG/SARS2 titers peaked at 48 hours following infection, the peak titer was orders of magniftude lower than peaks found with the other glycoproteins (Figure 2C).

3.2. Kinetics of rVSVΔG/VSV luciferase expression

Preprints (www.preprints.org) | NOT PEER-REVIEWED | Posted: 25 November 2020 doi:10.20944/preprints202011.0641.v1

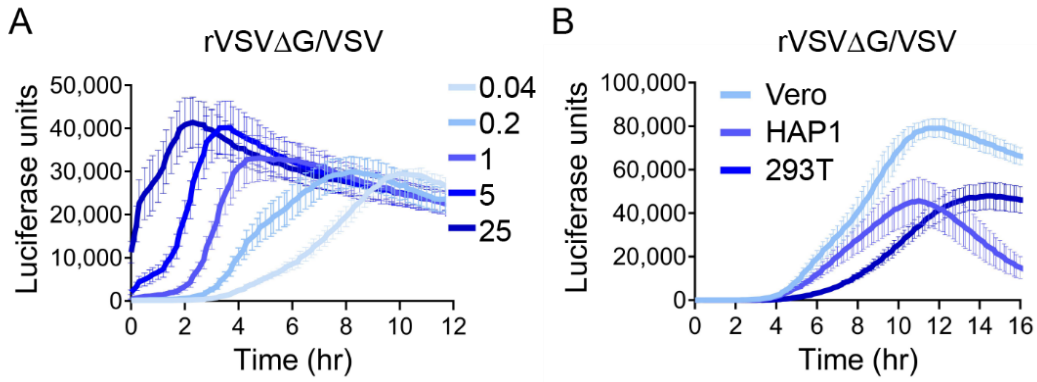

Figure 3. rVSVΔG/VSV entry kinetics. (**A**) VeroS cells were infected with rVSVΔG/VSV at multiple MOIs, inoculum was removed after 1 hr, and monitored for luciferase production overtime. (**B**) VeroS, HAP1, and HEK293T cells were infected with rVSVΔG/VSV (MOI 1), inoculum was not removed, and monitored for luciferase production overtime. Each experiment was repeated in duplicate, three independent times. Data shown are the averages and SEM.

To examine how quickly we can detect viral entry in our rVSV system, we used the live-cell luciferase substrate Endurazine™, which requires cellular esterase cleavage in order to react with the rVSV-encoded NLucP reporter gene and produce luminescence. We measured luminescence over a shorter time course than that of our replication curves in order to capture the first 1-2 rounds of replication. We first observed rVSV containing its native glycoprotein (G). VSV G is known to efficiently and quickly enter cells and fuse out of early endosomes [54]. We first assessed how changes in MOI values could impact the kinetics of luciferase expression of rVSVΔG/VSV, by infecting VeroS cells at a MOI of 25, 5, 1, 0.2, and 0.04. The virus was added to the cells for one hour, then both the inoculum and luciferase substrate were removed, and the cells were placed in the pre-warmed plate reader, therefore only particles that bound within the hour could initiate infection. At 1-hour post-infection, luciferase production from cells infected at the highest MOI (25) already displayed a signal value of ~10,000 units and quickly peaked 3 hours post-infection (Figure 3A). At a MOI of 5, the luciferase signal quickly increased and peaked 3.5 hours post-infection. When adding fewer particles to the cells we could detect a clear eclipse phase, with approximately 1 virus per cell (MOI 1) luciferase signal was detected about two hours after removal of the inoculum, and the signal rapidly rises and displayed a maximum peak at 5 hours post infection. This suggests the time from infection to peak protein production occurs within the 5 hours of infection, which is consistent with previous studies of VSV replication kinetics [54]. At lower MOI infections, we observed an almost steady increase in luciferase production, which peaked late, between 8-10 hours. We attribute this to virus spreading to uninfected cells, eventually exhausting the luciferase substrate.

To compare luciferase activity across different cell types, we seeded VeroS, HAP1, and HEK293T cells at the same cell density and infected them with rVSVΔG/VSV (MOI 1) (Figure 3B). Because HAP1 and HEK293T cells did not withstand washing, the viral inoculum was not removed in this experiment. When we compare the VeroS MOI 1 data between Figure 3A and 3B, we can see how different the luciferase signal accumulates when the inoculum is removed versus left on the cells. The data suggest additional virus continues to bind and enter cells throughout the course of the experiment, enabling more luciferase to be produced. In addition, the luciferase substrate was also present for the length of the infection in figure 3B, which was attributed to the higher peak values that were produced later in the infection. Within this experiment VeroS and HAP1 cells displayed similar initial signals and peak times (between 11- and 12-hours post-infection), however, VeroS cells reached a higher peak than HAP1 cells. Luciferase production in HEK293T was slower than in VeroS and HAP1 cells; it reached a similar peak value to the HAP1 cell line, but about 3 hours later (Figure 3B).

3.3. Kinetics of rVSVΔG/LASV luciferase expression

Preprints (www.preprints.org) | NOT PEER-REVIEWED | Posted: 25 November 2020 doi:10.20944/preprints202011.0641.v1

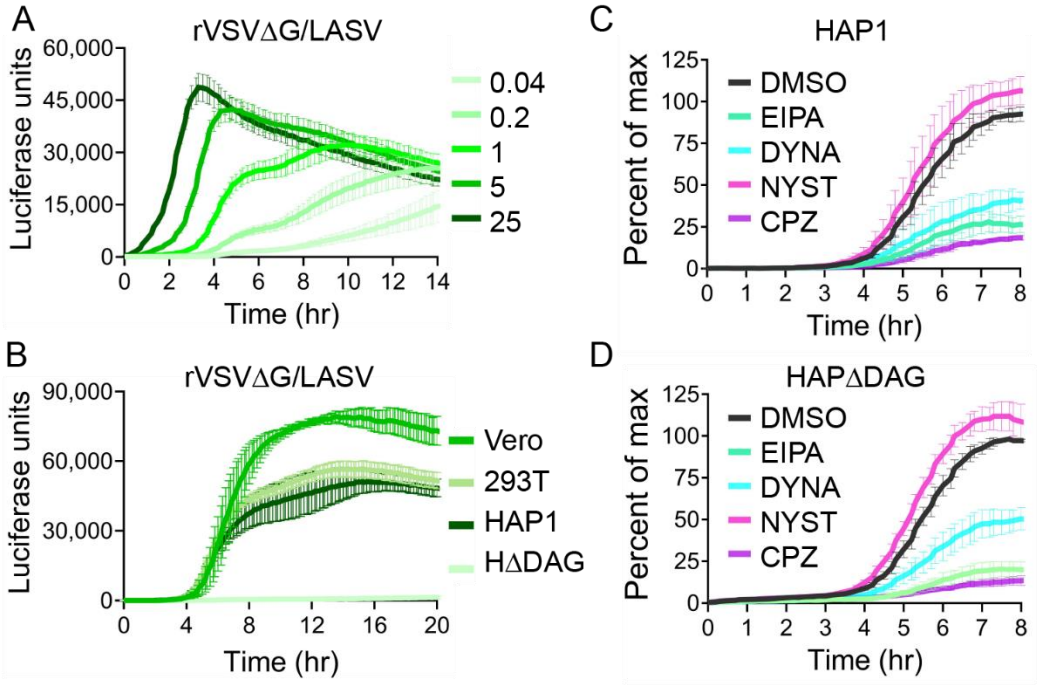

Figure 4. rVSVΔG/LASV entry kinetics: (**A**) VeroS cells were infected with rVSVΔG/LASV at multiple MOIs, inoculum was removed after 1 hr, and monitored for luciferase production overtime. (**B**) VeroS, HEK293T, HAP1, and HΔDAG cells were infected with rVSVΔG/LASV (MOI 1), inoculum was not removed, and monitored for luciferase production overtime. (**C**) HAP1 cells and (D) HΔDAG cells were infected with rVSVΔG/LASV (HΔDAG cells required 100 times as much virus) in the presence of commonly used entry inhibitors. Results are displayed as percentage of the maximum signal seen with mock treatment. Each experiment was repeated in duplicate, three independent times. Data shown are the averages and SEM.

Once we established how quickly we could detect luciferase signal when rVSV was entering using the VSV G, we compared how quickly rVSV entry occurs when the LASV GP is mediating entry. Unlike VSV G, which fuses with early endosomal membranes, LASV fusion requires low pH values found in late endosomes/lysosomes and therefore we predicted luciferase production would both start and peak at later time points than VSV G. To determine signal peak and relative strength, we infected VeroS cells at a MOI of 25, 5, 1, 0.2, and 0.5. While VSV G mediated entry at high MOI (25) peaked at two hours, LASV GP was slower and displayed a maximum signal peak at 3.5 hours (Figure 4A). At lower MOIs we detected a slight plateau in the signal accumulation between 5-7 hours after which a second round of infection induced more luciferase production (Figure 4A).

LASV GP interacts with αDG to efficiently enter cells, but can enter cells through additional attachment factors. We compared LASV entry into 293T and HAP1 cells which both produce αDG, as well as VeroS cells, which lack properly glycosylated αDG [12,16], and HAP1 cells knocked out for αDG gene (HΔDAG) (Figure 4B). Both HAP1 and HEK293T cell lines that contain αDG displayed overlapping kinetics of luciferase expression over the course of the experiment (Figure 4B). VeroS cells contain high levels of PtdSer receptors that facilitate LASV entry in the absence of αDG [16], and the rate of signal closely followed the αDG producing cells, but produced higher overall luciferase levels. The HΔDAG did not produce significant signal above background for the first 12 hours, but signal eventually separated from background although remained low.

Previous studies have demonstrated that rVSVΔG/LASV can enter HΔDAG cells if enough virus is added to the culture [15,46]. Despite the lack of αDG, we could detect similar levels of luciferase production in the HΔDAG1 by increasing the viral load by a 100-fold over the level added to HAP1 cells (Figure 4C and D). To determine if virion internalization occurs through similar or distinct mechanisms if particles interact with αDG or other attachment factors, we infected HAP1 and HΔDAG1 at a MOI of 1 and 100 respectively, and measured luminescence in the presence of

Preprints (www.preprints.org) | NOT PEER-REVIEWED | Posted: 25 November 2020 doi:10.20944/preprints202011.0641.v1

chlorpromazine, EIPA, dynasore, or nystatin entry inhibitors (Figure 4C and D). After normalization to control (DMSO), both HAP1 and HΔDAG1 cells displayed similar patterns of inhibition. Viral entry into both cell types is strongly inhibited by macropinocytosis (EIPA) and clathrin-mediated (CPZ) endocytosis inhbitors, but is not affected by nystatin which blocks caveolin internalization.

3.5. Kinetics of rVSVΔG/EBOV luciferase expression

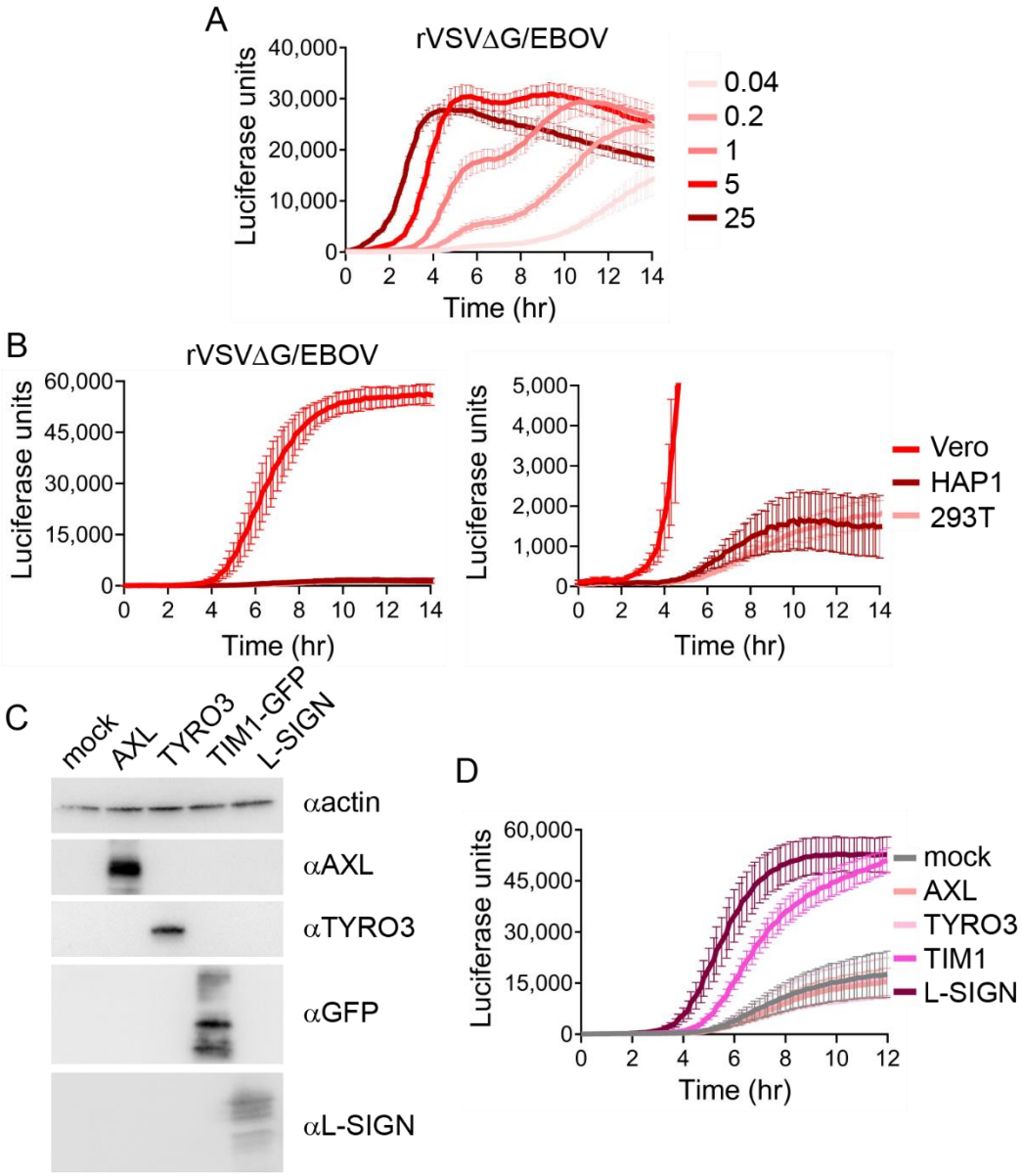

Figure 5. rVSVΔG/EBOV entry kinetics: (**A**) VeroS cells were infected with rVSVΔG/EBOV at multiple MOIs, inoculum was removed after 1 hr, and monitored for luciferase production overtime. (**B**) VeroS, HEK293T, and HAP1 cells were infected with rVSVΔG/EBOV (MOI 1), inoculum was not removed, and monitored for luciferase production overtime. Right panel zooms in to display the signals observed in HAP1 and HEK293T cells. (**C**) Immunoblots demonstrating production of the transfected receptors in HEK293T cells. (**D**) HEK293T cells transfected with the indicated receptors were infected with rVSVΔG/EBOV and monitored for luciferase production overtime. Each experiment was repeated in duplicate, three independent times. Data shown are the averages and SEM.

Next, we examined rVSVΔG/EBOV entry. Like LASV, EBOV entry requires virions to traffic into more mature endosomes before fusion can occur. EBOV must first undergo proteolytic cleavage by

Preprints (www.preprints.org) | NOT PEER-REVIEWED | Posted: 25 November 2020 doi:10.20944/preprints202011.0641.v1

endosomal cathepsins before it can interact with the endosomal receptor NPC1 [25,26]. Infection of VeroS cells with rVSVΔG/EBOV at a MOI of 25 (PFU/cell), resulted in a signal peak at 4.5 hours post-infection and at a MOI of 1 the signal peaked around 7 hours (Figure 5A), and therefore slower than both VSV G and LASV GP mediated entry.

rVSVΔG/EBOV infection of HAP1 and HEK293T yielded comparably low luciferase activity to VeroS cells (Figure 5B). While the signals were less than 4% of that observed in VeroS cells, the signal peaks were reached between 10-12 hours following infection. Previous reports suggest HEK293Ts are not highly permissive for EBOV entry [22], yet the NPC1 receptor was identified by infecting HAP1 cells with rVSVΔG/EBOV [26]. Attachment factors play a key role in the facilitation of EBOV entry [22-24]. Since HEK293T cells naturally lack PtdSer receptors and C-type lectins, we wanted to evaluate whether luciferase signal could be enhanced by producing attachment factors. We transfected HEK293Ts with plasmids encoding L-SIGN, Axl, Tyro3, and TIM-1-GFP and confirmed protein production with immunoblots (Figure 5C). Our results indicate that HEK293T cells transfected with L-SIGN and TIM-1-GFP, reached a higher signal value upon rVSVΔG/EBOV infection in comparison to control group, with signals peaking first when L-SIGN was present (Figure 5D). In contrast, HEK293T cells transfected with Axl and Tyro3 remained at baseline level and no significant change was observed.

3.6. Kinetics of rVSVΔG/SARS2 luciferase expression

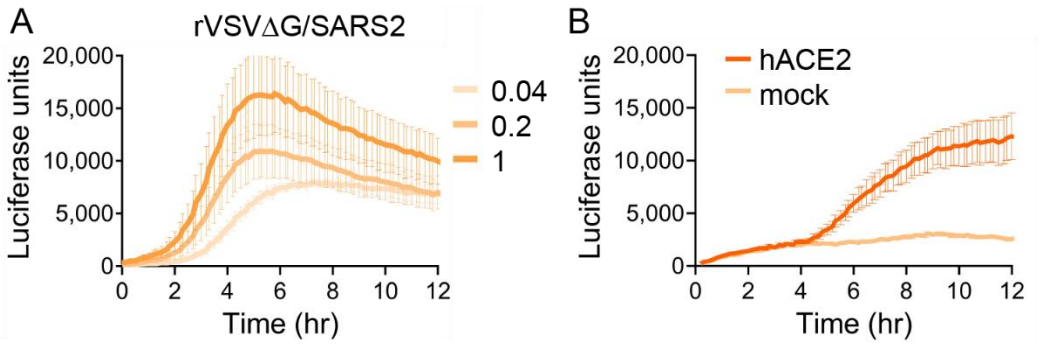

Figure 6. rVSVΔG/SARS2 entry kinetics: (**A**) VeroS cells were infected with rVSVΔG/SARS2 at multiple MOIs, inoculum was removed after 1 hr, and monitored for luciferase production overtime. (**B**) HEK293T were either mock transfected or transfected with ACE2 and infected with rVSVΔG/SARS2 and luciferase production was monitored overtime. Each experiment was repeated in duplicate, three independent times. Data shown are the averages and SEM.

rVSVΔG/SARS2 did not replicate to the high titers seen with the other glycoproteins and therefore we were unable to achieve the high MOI infections. Titers permitted infections at an MOI of 1, and signal accumulated relatively fast, peaking at 5 hours post infection (Figure 6A) At lower MOIs we did not observe a second wave of luciferase produced as seen with EBOV and LASV (Figures 4A and 5A), which may relate to the poor titers produced with rVSVΔG/SARS2 (Figure 2C).

SARS2 S protein interacts with ACE2 to facilitate entry into cells [7]. By transiently producing ACE2 in 293T cells which naturally lack ACE2 expression, we can detect significant luciferase signal compared to background levels starting at 5 hours following infection (Figure 6B). rVSVΔG/SARS2 particles did display higher background signal than the other rVSV. We attribute this to the low titers which required higher volumes of inoculum to be added to the experiment.

3.7. Kinetics of rVSVΔG/CHIKV and CHIKV luciferase expression

Preprints (www.preprints.org) | NOT PEER-REVIEWED | Posted: 25 November 2020 doi:10.20944/preprints202011.0641.v1

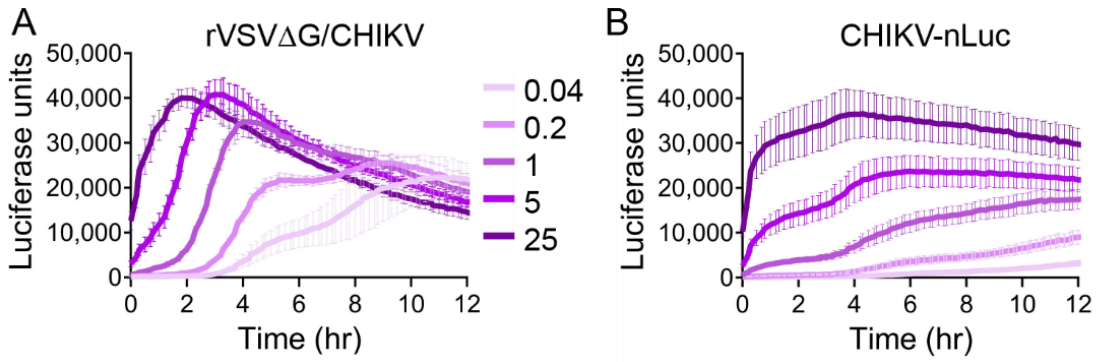

Figure 7. rVSVΔG/CHIK and CHIKV entry kinetics. VeroS cells were infected with rVSVΔG/CHIKV (**A**) or CHIKV (**B**) at multiple MOIs, inoculum was removed after 1 hr and monitored for luciferase production overtime. Each experiment was repeated in duplicate, three independent times. Data shown are the averages and SEM.

We performed the same multi MOI experiment on VeroS cells utilizing rVSV expressing the wild type CHIKV envelope (S27), and compared the rVSV signals to CHIKV (181/c25) that produces nano luciferase from a subgenomic RNA. rVSVΔG/CHIKV luciferase kinetics closely mirrored rVSVΔG/VSV with signals rapidly increasing and peaking at 4 hours post-infection at an MOI 1. The two lowest MOIs (0.2 and 0.04), display a multistep curve, suggesting the first round of replication peaks at about 5 hours post-infection followed by a second peak approximately 5 hours later (Figure 7A). CHIKV-nLuc curves followed different trends than the rVSV. Altering the amount of virus in the inoculum caused a clear difference in signal (Figure 7B). While the time frame for rVSV genome to accumulate luciferase signal was a few hours, CHIKV-nLuc signals rapidly produced signal within 1 hour of infection. That signal remained relatively stable until 4 hours post-infection when an increase in signal produced was observed.

3.8. Comparative analysis of rVSV viruses' kinetics of luciferase expression

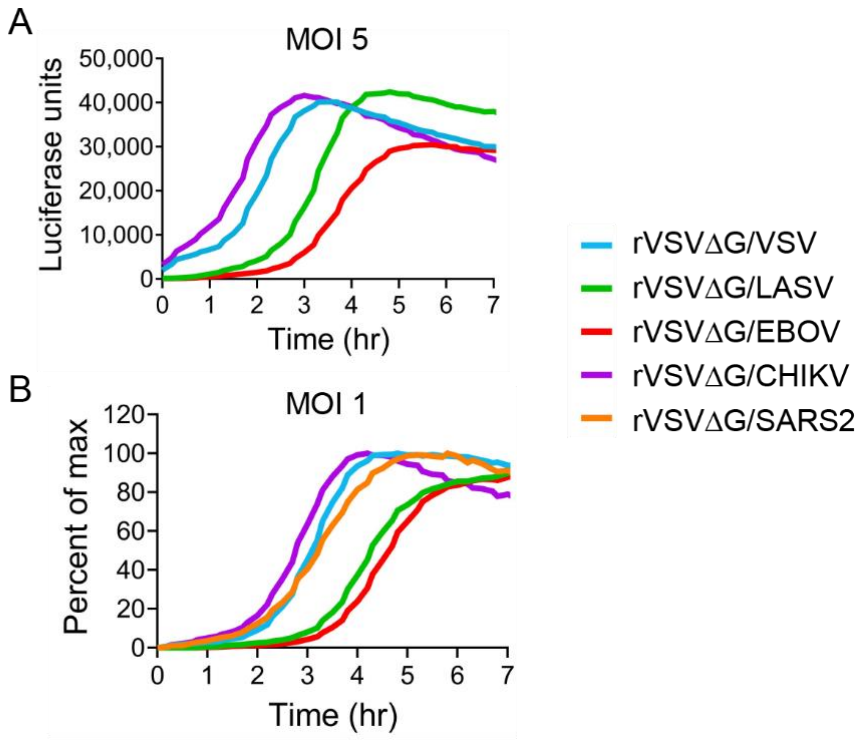

Preprints (www.preprints.org) | NOT PEER-REVIEWED | Posted: 25 November 2020 doi:10.20944/preprints202011.0641.v1

Figure 8. Comparative analysis of rVSV viruses. Data displayed in Figures 3-7 were replotted to compare the entry kinetics of the five viruses. MOI 5 data is displayed (**A**). To compare time to peak, the data at MOI 1 was replotted as percent of max (**B**).

To compare all the rVSV viruses, we overlayed the luciferase signals produced at high MOI (5) (Figure 8A). Surprisingly CHIKV envelope mediated entry induced slightly faster luciferase signals than even the native VSV glycoprotein. Both LASV and EBOV mediated signals peaked more than an hour later. To compare all five glycoproteins, we focused on the time it took to reach peak signal at MOI 1 (Figure 8B). EBOV and LASV mediated luciferase signals peak later in the infection, whereas VSV, CHIK and SARS2 are able to produce higher luciferase signals earlier in the infection.

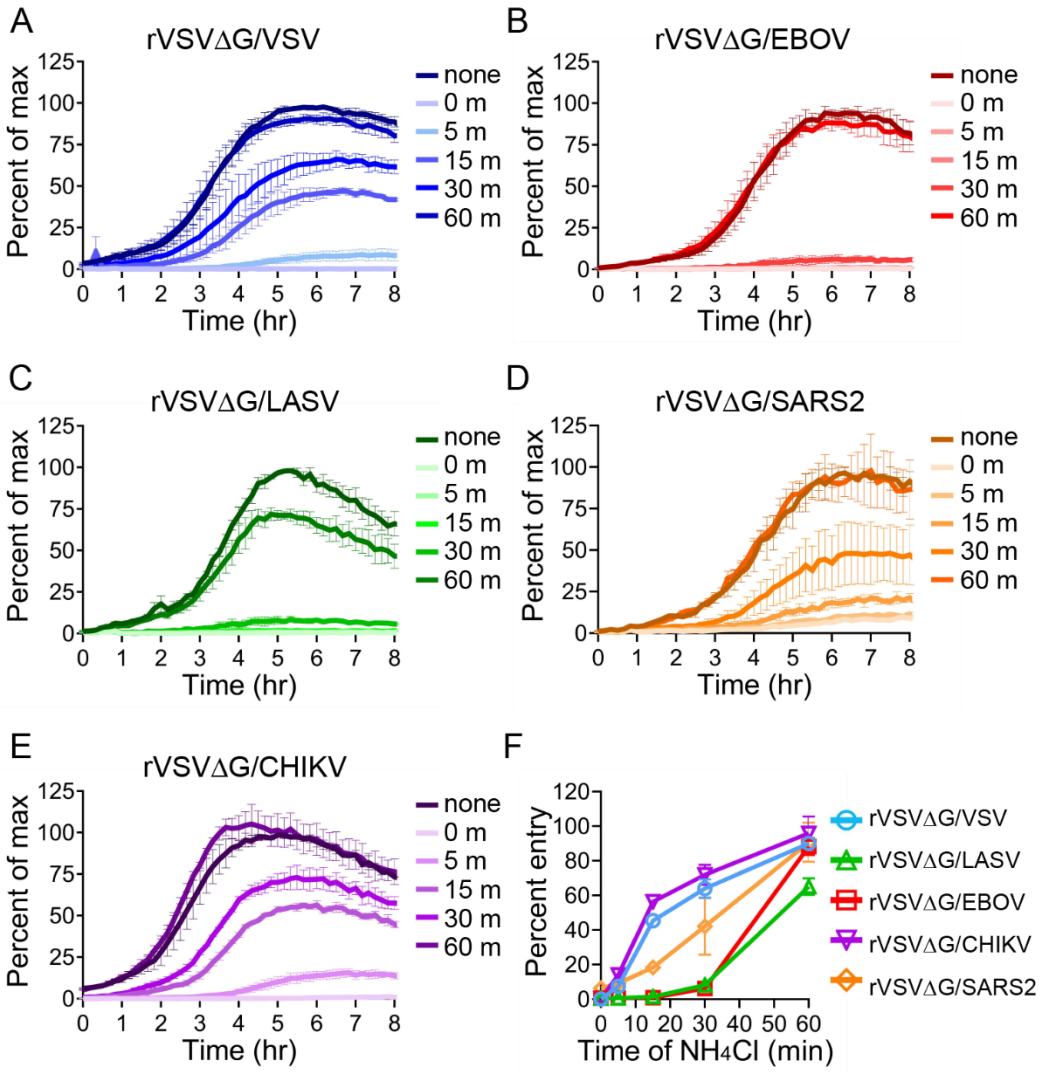

Figure 9. rVSV entry in presence of ammonium chloride. VeroS cells were infected with (**A**) rVSVΔG/VSV, (**B**) rVSVΔG/EBOV, (**C**) rVSVΔG/LASV, (**D**) rVSVΔG/CHIKV, and (**E**) rVSVΔG/SARS2 (MOI 1). At the indicated time points ammonium chloride was added to prevent low pH mediated fusion. One-hour post infection the inoculum was removed and luciferase production was monitored overtime. (**F**) Percent of max luciferase produced 6 hours post-infection was plotted to compare how quickly the different glycoproteins escape the ammonium chloride entry block. Each experiment was repeated in duplicate, three independent times. Data shown are the averages and SEM.

In all of these experiments, luciferase is produced by the viral replication machinery after the internal VSV ribonucleoprotein complex is delivered into the cytoplasm following membrane fusion. Because the five glycoproteins range in size, (e.g. SARS2 S protein is more than twice the size of VSV G), we wanted to confirm that the delay in luciferase production correlated to the virions fusing with

Preprints (www.preprints.org) | NOT PEER-REVIEWED | Posted: 25 November 2020 doi:10.20944/preprints202011.0641.v1

the endosomal membrane. All five of the glycoproteins enter VeroS cells through an endosomal route, and fusion is triggered through low pH dependent processes [9,20,25,55,56]. Therefore we infected VeroS cells at MOI 1 and added ammonium chloride (NH_4Cl), a lysosomotropic agent, that quickly prevents endosomal acidification and should prevent luciferase production if the virions have not undergone fusion. Adding NH_4Cl at the time of infection prevented luciferase production for all viral glycoproteins (Figure 9). Both VSV and CHIKV fusion occurred quickly, with approximately half of the particles escaping the NH_4Cl block within 15 minutes (Figure 9A and E). SARS2 required 30 minutes (Figure 9D) for half of the particles to escape the endosomal compartment. Both EBOV and LASV displayed a much slower entry pathway, with the majority of particles being blocked when adding NH_4Cl 30 minutes after infection (Figure 9B and C). The percent of entry observed at 6 hours post infections was plotted to compare the five glycoproteins. Similar to the previous experiments, VSV and CHIKV had faster fusion kinetics, followed by SARS2, and lastly EBOV, and LASV (Figure 9F).

3.9. rVSVΔG/EBOV kinetics of luciferase expression shifts with thermolysin treatment

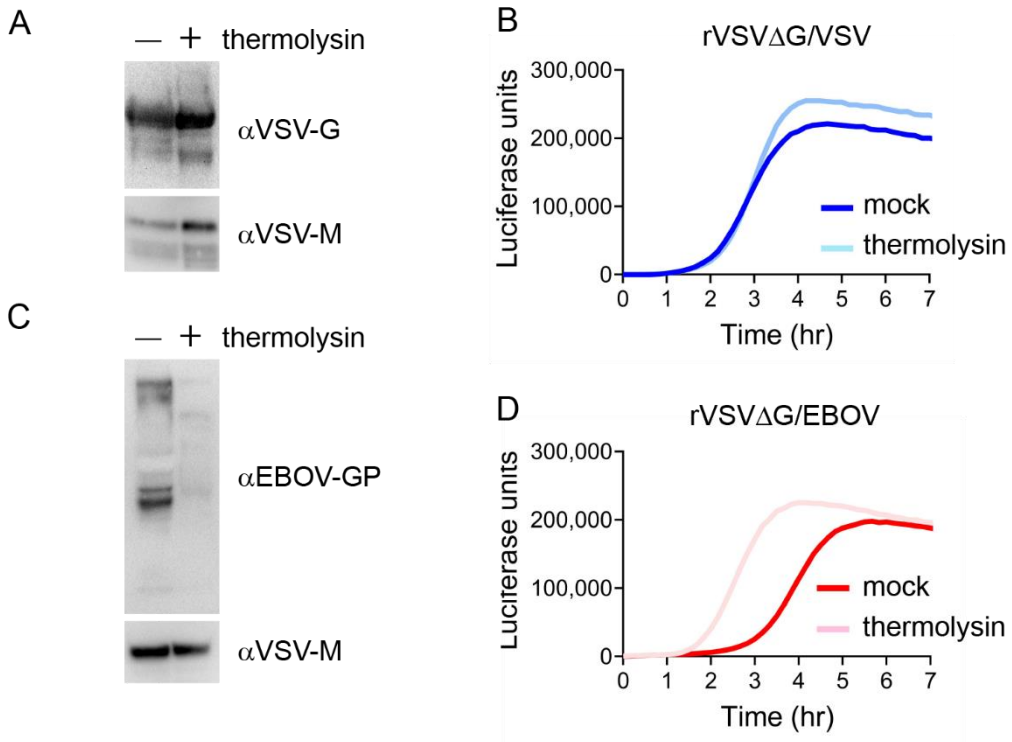

Figure 10. rVSVΔG/EBOV entry occurs faster with proteolytically processing GP. Immunoblots of rVSVΔG/VSV (**A**) or rVSVΔG/EBOV (**C**) treated or mock-treated with thermolysin. VeroS cells were infected with rVSVΔG/VSV (**B**) or rVSVΔG/EBOV (**D**) treated or mock-treated with thermolysin and luciferase production was monitored overtime. The experiments were repeated in duplicate, three independent times. A representative experiment is shown.

rVSVΔG/EBOV entry required significantly more time than rVSVΔG/VSV. While rVSVΔG/VSV can be triggered by exposure to low pH, EBOV GP must undergo proteolytic processing in the late endosomes before it can interact with its receptor and trigger fusion [25]. EBOV GP proteolysis can be mimicked by treating the viral particles with thermolysin, a metallopeptidase [57]. To determine if cathepsin cleavage is a rate-limiting factor in the entry kinetics of EBOV GP we treated either rVSVΔG/VSV or rVSVΔG/EBOV particles with thermolysin before infecting cells and monitoring luciferase activity. While thermolysin treatment did not alter VSV G levels on the particle, thermolysin decreased the levels of full-length EBOV GP (Figure 10A and C). Unfortunately, our EBOV GP antibody did not appear to detect the 19kDa GP fragment. Thermolysin treatment did not alter virion titers and both untreated and treated rVSVΔG/VSV particles produced luciferase levels

 doi:10.20944/preprints202011.0641.v1

at similar rates (Figure 10B). Thermolysin treated rVSVΔG/EBOV particles displayed a shift in luciferase production, with treated particles producing luciferase two hours earlier than untreated particles and similarly reaching signal peak two hours earlier (Figure 10D).

4. Discussion

The production of replication competent chimeric VSV particles has been used extensively to examine virus entry of highly pathogenic viruses in a BLS2 system [58-60]. These particles are also being used as vaccine vectors, with the rVSV-ZEBOV becoming the first licensed EBOV vaccine [61,62]. We employed this system to compare the efficiencies of different viral glycoproteins in live cells. All of the viruses contain the same internal VSV replication machinery and only differ in the outer glycoprotein. Therefore, we monitored the production on a NlucP reporter construct as a surrogate for virus entry, assuming that the VSV machinery would have similar transcription kinetics once the viral core was delivered to the cytoplasm. VSV G, CHIKV E, and SARS-CoV-2 S mediated entry at a faster rate than EBOV and LASV. Although the genome length varied among the viruses (Figure 1A), the differences in length did not correlate with changes in luciferase production, suggesting that the additional length did not significantly alter the rate of luciferase production. The CHIKV E protein open reading frame is about twice the length of the VSV G, yet both viruses mediated luciferase production at very similar rates (Figure 3A and 7A). Additionally, the time frame observed monitoring luciferase production closely correlated with the time-of-addition assays that blocked low pH-dependent fusion. VSV G and CHIK E particles were able to escape the low pH step in viral entry at a faster rate than SARS-CoV-2 S, which was faster than the comparatively slow entry mediated by LASV GP and EBOV GP.

While all five viral glycoproteins require low pH for entry, LASV GP and EBOV GP require endosomal receptor binding and EBOV GP requires proteolytic processing [15,20]. Because we observed that rVSVΔG/EBOV entry was slower than rVSVΔG/LASV entry, we examined if EBOV GP proteolytic processing delays rVSVΔG/EBOV entry. We pre-cleaved rVSVΔG/EBOV particles with thermolysin and found that pre-cleaved particles produced luciferase significantly earlier than non-cleaved particles, suggesting proteolysis is a rate-limiting step in EBOV entry. SARS-CoV-2 S also requires proteolytic cleavage, either at the plasma membrane or in endosomes. Here we infected VeroS cells, which lack TMPRSS2, a cell surface protease required for S cleavage at the plasma membrane [7,8]. However, cathepsins found in the endosomal compartments can compensate, enabling entry [9,10]. With both EBOV and SARS-CoV-2 requiring endosomal cathepsin cleavage to initiate fusion in our system, we were surprised that SARS-CoV-2 entry occurred at a faster rate than EBOV. In addition to EBOV GP needing to interact with NPC1 following cathepsins cleavage, additional, undefined steps are needed to trigger EBOV GP [26,53,63], whereas for SARS-CoV-2 S proteolysis is the primary trigger of S conformational changes.

SARS-CoV-2 Spike-containing rVSV particles poorly spread in our multi-step replication curves and produced significantly lower titers than the other chimeric viruses. Surprisingly, the first round of entry was comparably efficient and produced luciferase as quickly as rVSV/VSV; however, we did not observe a second wave of luciferase production. This may be due to poor SARS-CoV-2 S incorporation onto particles.

We compared rVSVΔG/VSV, rVSVΔG/EBOV, and rVSVΔG/LASV entry in VeroS, HAP1 and HEK293T cells. With all three viruses, infection in VeroS cells resulted in significantly higher luciferase levels, whereas luciferase production in HEK293T and HAP1 were equally reduced (Figure 3B, 4B and 5B). Both rVSVΔG/VSV and rVSVΔG/LASV entered all three cell types with similar efficiencies, suggesting the higher overall luciferase values in VeroS cells may be attributed to other factors such as increased cell size (each VeroS cell is approximately twice as large as a HAP1 or HEK293T cell) or greater VeroS Endurazine™ processing. The high sensitivity of NlucP-Enduazine™ system enabled the detection of virus replication even when very few particles were efficiently entering (Figure 4B and 5B), suggesting that a slight increase in VeroS Endurazine processing may result in greater amplified luciferase signals.

We also compared rVSVΔG/CHIK and CHIKV entry efficiencies. Cells infected with CHIKV produced luciferase activity more rapidly than rVSVΔG/CHIK and rVSVΔG/VSV, which is likely due to CHIKV's positive sense RNA genome. The initial spike in luciferase from the first round of CHIKV replication remained relatively stable for three hours, after which a second round of replication was detected by an increase in luciferase activity (Figure 7B). rVSVΔG/CHIK, which contains a non-native glycoprotein and a negative-sense RNA genome, produced luciferase at a slower rate (Figure 7A). Luminescence also continued to increase throughout the first round of rVSVΔG/CHIK infection, rather than remaining relatively stable as seen with CHIKV. One caveat when comparing the data, the rVSV encoded for NLucP includes a PEST protein degradation domain to reduce background from virus inoculum and ensure the protein is actively being produced during the assay. CHIKV-NLuc does not contain the PEST domain, so the rapid signal with little accumulation over the first three hours may be due to the high activity and low turnover of NLuc in this viral infection. Future comparisons should include the same NLucP reporter in both viruses.

5. Conclusions

In conclusion, we can use rVSV viruses to compare the entry kinetics from a wide range of viral glycoproteins. This live-cell assay quickly enables one to compare viral entry conditions in various cell lines and is highly sensitive. The method could easily be adapted for screening purposes.

Acknowledgments

Research reported in this publication was supported by the National Institute of Allergy and Infectious Diseases of the National Institutes of Health under Award Number R01AI139238. The content is solely the responsibility of the authors and does not necessarily represent the official views of the National Institutes of Health.

Author Contributions

Conceptualization, M.A.B. and M.F.L.; Methodology, M.A.B. and M.F.L.; Formal Analysis, M.A.B. and M.F.L.; Investigation, M.F.L., M.D.A., C.N.L., C.S.M., and M.A.B.; Data Curation, M.F.L.; Writing – Original Draft Preparation, M.F.L.; Writing – Review & Editing, M.F.L., M.D.A., M.A.B.; Visualization, M.F.L.; Supervision, M.A.B.; Project Administration, M.A.B.; Funding Acquisition, M.A.B.

Conflicts of Interest

The authors declare no conflict of interest.

References

1. Plemper, R.K. Cell entry of enveloped viruses. *Curr Opin Virol* **2011**, *1*, 92-100, doi:10.1016/j.coviro.2011.06.002.
2. White, J.M.; Delos, S.E.; Brecher, M.; Schornberg, K. Structures and mechanisms of viral membrane fusion proteins: multiple variations on a common theme. *Crit Rev Biochem Mol Biol* **2008**, *43*, 189-219, doi:10.1080/10409230802058320.
3. Cosset, F.L.; Lavillette, D. Cell entry of enveloped viruses. *Adv Genet* **2011**, *73*, 121-183, doi:10.1016/B978-0-12-380860-8.00004-5.
4. Xu, Y.; Liu, Y.; Lou, Z.; Qin, L.; Li, X.; Bai, Z.; Pang, H.; Tien, P.; Gao, G.F.; Rao, Z. Structural basis for coronavirus-mediated membrane fusion. Crystal structure of mouse hepatitis virus spike protein fusion core. *J Biol Chem* **2004**, *279*, 30514-30522, doi:10.1074/jbc.M403760200.

5. Wrapp, D.; Wang, N.S.; Corbett, K.S.; Goldsmith, J.A.; Hsieh, C.L.; Abiona, O.; Graham, B.S.; McLellan, J.S. Cryo-EM structure of the 2019-nCoV spike in the prefusion conformation. *Science* **2020**, *367*, 1260-+, doi:10.1126/science.abb2507.
6. Zhou, P.; Yang, X.L.; Wang, X.G.; Hu, B.; Zhang, L.; Zhang, W.; Si, H.R.; Zhu, Y.; Li, B.; Huang, C.L., et al. A pneumonia outbreak associated with a new coronavirus of probable bat origin. *Nature* **2020**, *579*, 270-+, doi:10.1038/s41586-020-2012-7.
7. Hoffmann, M.; Kleine-Weber, H.; Schroeder, S.; Kruger, N.; Herrler, T.; Erichsen, S.; Schiergens, T.S.; Herrler, G.; Wu, N.H.; Nitsche, A., et al. SARS-CoV-2 Cell Entry Depends on ACE2 and TMPRSS2 and Is Blocked by a Clinically Proven Protease Inhibitor. *Cell* **2020**, *181*, 271-280 e278, doi:10.1016/j.cell.2020.02.052.
8. Bestle, D.; Heindl, M.R.; Limburg, H.; Van Lam van, T.; Pilgram, O.; Moulton, H.; Stein, D.A.; Hardes, K.; Eickmann, M.; Dolnik, O., et al. TMPRSS2 and furin are both essential for proteolytic activation of SARS-CoV-2 in human airway cells. *Life Sci Alliance* **2020**, *3*, doi:10.26508/lsa.202000786.
9. Ou, X.; Liu, Y.; Lei, X.; Li, P.; Mi, D.; Ren, L.; Guo, L.; Guo, R.; Chen, T.; Hu, J., et al. Characterization of spike glycoprotein of SARS-CoV-2 on virus entry and its immune cross-reactivity with SARS-CoV. *Nat Commun* **2020**, *11*, 1620, doi:10.1038/s41467-020-15562-9.
10. Simmons, G.; Gosalia, D.N.; Rennekamp, A.J.; Reeves, J.D.; Diamond, S.L.; Bates, P. Inhibitors of cathepsin L prevent severe acute respiratory syndrome coronavirus entry. *Proc Natl Acad Sci U S A* **2005**, *102*, 11876-11881, doi:10.1073/pnas.0505577102.
11. Cao, W.; Henry, M.D.; Borrow, P.; Yamada, H.; Elder, J.H.; Ravkov, E.V.; Nichol, S.T.; Compans, R.W.; Campbell, K.P.; Oldstone, M.B.A. Identification of α-Dystroglycan as a Receptor for Lymphocytic Choriomeningitis Virus and Lassa Fever Virus. *Science* **1998**, *282*, 2079-2081.
12. Kunz, S.; Rojek, J.M.; Kanagawa, M.; Spiropoulou, C.F.; Barresi, R.; Campbell, K.P.; Oldstone, M.B. Posttranslational modification of alpha-dystroglycan, the cellular receptor for arenaviruses, by the glycosyltransferase LARGE is critical for virus binding. *J Virol* **2005**, *79*, 14282-14296, doi:10.1128/JVI.79.22.14282-14296.2005.
13. Shimojima, M.; Stroher, U.; Ebihara, H.; Feldmann, H.; Kawaoka, Y. Identification of cell surface molecules involved in dystroglycan-independent Lassa virus cell entry. *J Virol* **2012**, *86*, 2067-2078, doi:10.1128/JVI.06451-11.
14. Goncalves, A.R.; Moraz, M.L.; Pasquato, A.; Helenius, A.; Lozach, P.Y.; Kunz, S. Role of DC-SIGN in Lassa virus entry into human dendritic cells. *J Virol* **2013**, *87*, 11504-11515, doi:10.1128/JVI.01893-13.
15. Jae, L.T.; Raaben, M.; Herbert, A.S.; Kuehne, A.I.; Wirchnianski, A.S.; Soh, T.K.; Stubbs, S.H.; Janssen, H.; Damme, M.; Saftig, P., et al. Virus entry. Lassa virus entry requires a trigger-induced receptor switch. *Science* **2014**, *344*, 1506-1510, doi:10.1126/science.1252480.
16. Brouillette, R.B.; Phillips, E.K.; Patel, R.; Mahauad-Fernandez, W.; Moller-Tank, S.; Rogers, K.J.; Dillard, J.A.; Cooney, A.L.; Martinez-Sobrido, L.; Okeoma, C., et al. TIM-1 Mediates Dystroglycan-Independent Entry of Lassa Virus. *J Virol* **2018**, *92*, doi:10.1128/JVI.00093-18.
17. Fedeli, C.; Torriani, G.; Galan-Navarro, C.; Moraz, M.L.; Moreno, H.; Gerold, G.; Kunz, S. Axl Can Serve as Entry Factor for Lassa Virus Depending on the Functional Glycosylation of Dystroglycan. *J Virol* **2018**, *92*, doi:10.1128/JVI.01613-17.
18. Li, S.; Sun, Z.; Pryce, R.; Parsy, M.L.; Fehling, S.K.; Schlie, K.; Siebert, C.A.; Garten, W.; Bowden, T.A.; Strecker, T., et al. Acidic pH-Induced Conformations and LAMP1 Binding of the Lassa Virus Glycoprotein Spike. *PLoS Pathog* **2016**, *12*, e1005418, doi:10.1371/journal.ppat.1005418.

19. Cosset, F.L.; Marianneau, P.; Verney, G.; Gallais, F.; Tordo, N.; Pecheur, E.I.; ter Meulen, J.; Deubel, V.; Bartosch, B. Characterization of Lassa virus cell entry and neutralization with Lassa virus pseudoparticles. *J Virol* **2009**, *83*, 3228-3237, doi:10.1128/JVI.01711-08.
20. Bulow, U.; Govindan, R.; Munro, J.B. Acidic pH Triggers Lipid Mixing Mediated by Lassa Virus GP. *Viruses* **2020**, *12*, doi:10.3390/v12070716.
21. Hunt, C.L.; Kolokoltsov, A.A.; Davey, R.A.; Maury, W. The Tyro3 receptor kinase Axl enhances macropinocytosis of Zaire ebolavirus. *J Virol* **2011**, *85*, 334-347, doi:10.1128/JVI.01278-09.
22. Kondratowicz, A.S.; Lennemann, N.J.; Sinn, P.L.; Davey, R.A.; Hunt, C.L.; Moller-Tank, S.; Meyerholz, D.K.; Rennert, P.; Mullins, R.F.; Brindley, M., et al. T-cell immunoglobulin and mucin domain 1 (TIM-1) is a receptor for Zaire Ebolavirus and Lake Victoria Marburgvirus. *Proc Natl Acad Sci U S A* **2011**, *108*, 8426-8431, doi:10.1073/pnas.1019030108.
23. Shimojima, M.; Takada, A.; Ebihara, H.; Neumann, G.; Fujioka, K.; Irimura, T.; Jones, S.; Feldmann, H.; Kawaoka, Y. Tyro3 family-mediated cell entry of Ebola and Marburg viruses. *J Virol* **2006**, *80*, 10109-10116, doi:10.1128/JVI.01157-06.
24. Alvarez, C.P.; Lasala, F.; Carrillo, J.; Muniz, O.; Corbi, A.L.; Delgado, R. C-type lectins DC-SIGN and L-SIGN mediate cellular entry by Ebola virus in cis and in trans. *J Virol* **2002**, *76*, 6841-6844, doi:10.1128/jvi.76.13.6841-6844.2002.
25. Chandran, K.; Sullivan, N.J.; Felbor, U.; Whelan, S.P.; Cunningham, J.M. Endosomal proteolysis of the Ebola virus glycoprotein is necessary for infection. *Science* **2005**, *308*, 1643-1645, doi:10.1126/science.1110656.
26. Carette, J.E.; Raaben, M.; Wong, A.C.; Herbert, A.S.; Obernosterer, G.; Mulherkar, N.; Kuehne, A.I.; Kranzusch, P.J.; Griffin, A.M.; Ruthel, G., et al. Ebola virus entry requires the cholesterol transporter Niemann-Pick C1. *Nature* **2011**, *477*, 340-343, doi:10.1038/nature10348.
27. Kielian, M.; Rey, F.A. Virus membrane-fusion proteins: more than one way to make a hairpin. *Nat Rev Microbiol* **2006**, *4*, 67-76, doi:10.1038/nrmicro1326.
28. Hoornweg, T.E.; van Duijl-Richter, M.K.S.; Ayala Nunez, N.V.; Albulescu, I.C.; van Hemert, M.J.; Smit, J.M. Dynamics of Chikungunya Virus Cell Entry Unraveled by Single-Virus Tracking in Living Cells. *J Virol* **2016**, *90*, 4745-4756, doi:10.1128/JVI.03184-15.
29. Carnec, X.; Meertens, L.; Dejarnac, O.; Perera-Lecoin, M.; Hafirassou, M.L.; Kitaura, J.; Ramdasi, R.; Schwartz, O.; Amara, A. The Phosphatidylserine and Phosphatidylethanolamine Receptor CD300a Binds Dengue Virus and Enhances Infection. *J Virol* **2016**, *90*, 92-102, doi:10.1128/JVI.01849-15.
30. Moller-Tank, S.; Kondratowicz, A.S.; Davey, R.A.; Rennert, P.D.; Maury, W. Role of the phosphatidylserine receptor TIM-1 in enveloped-virus entry. *J Virol* **2013**, *87*, 8327-8341, doi:10.1128/JVI.01025-13.
31. Silva, L.A.; Khomandiak, S.; Ashbrook, A.W.; Weller, R.; Heise, M.T.; Morrison, T.E.; Dermody, T.S. A single-amino-acid polymorphism in Chikungunya virus E2 glycoprotein influences glycosaminoglycan utilization. *J Virol* **2014**, *88*, 2385-2397, doi:10.1128/JVI.03116-13.
32. Wintachai, P.; Wikan, N.; Kuadkitkan, A.; Jaimipuk, T.; Ubol, S.; Pulmanausahakul, R.; Auewarakul, P.; Kasinrerk, W.; Weng, W.Y.; Panyasrivanit, M., et al. Identification of prohibitin as a Chikungunya virus receptor protein. *J Med Virol* **2012**, *84*, 1757-1770, doi:10.1002/jmv.23403.
33. Zhang, R.; Kim, A.S.; Fox, J.M.; Nair, S.; Basore, K.; Klimstra, W.B.; Rimkunas, R.; Fong, R.H.; Lin, H.; Poddar, S., et al. Mxra8 is a receptor for multiple arthritogenic alphaviruses. *Nature* **2018**, *557*, 570-574, doi:10.1038/s41586-018-0121-3.

34. Roche, S.; Rey, F.A.; Gaudin, Y.; Bressanelli, S. Structure of the prefusion form of the vesicular stomatitis virus glycoprotein G. *Science* **2007**, *315*, 843-848, doi:10.1126/science.1135710.
35. Roche, S.; Bressanelli, S.; Rey, F.A.; Gaudin, Y. Crystal structure of the low-pH form of the vesicular stomatitis virus glycoprotein G. *Science* **2006**, *313*, 187-191, doi:10.1126/science.1127683.
36. Heldwein, E.E.; Lou, H.; Bender, F.C.; Cohen, G.H.; Eisenberg, R.J.; Harrison, S.C. Crystal structure of glycoprotein B from herpes simplex virus 1. *Science* **2006**, *313*, 217-220, doi:10.1126/science.1126548.
37. Kadlec, J.; Loureiro, S.; Abrescia, N.G.; Stuart, D.I.; Jones, I.M. The postfusion structure of baculovirus gp64 supports a unified view of viral fusion machines. *Nat Struct Mol Biol* **2008**, *15*, 1024-1030, doi:10.1038/nsmb.1484.
38. Gaudin, Y. Reversibility in fusion protein conformational changes. The intriguing case of rhabdovirus-induced membrane fusion. *Subcell Biochem* **2000**, *34*, 379-408, doi:10.1007/0-306-46824-7_10.
39. Fan, D.P.; Sefton, B.M. The entry into host cells of Sindbis virus, vesicular stomatitis virus and Sendai virus. *Cell* **1978**, *15*, 985-992, doi:10.1016/0092-8674(78)90282-9.
40. Superti, F.; Seganti, L.; Ruggeri, F.M.; Tinari, A.; Donelli, G.; Orsi, N. Entry pathway of vesicular stomatitis virus into different host cells. *J Gen Virol* **1987**, *68 (Pt 2)*, 387-399, doi:10.1099/0022-1317-68-2-387.
41. Finkelshtein, D.; Werman, A.; Novick, D.; Barak, S.; Rubinstein, M. LDL receptor and its family members serve as the cellular receptors for vesicular stomatitis virus. *Proc Natl Acad Sci U S A* **2013**, *110*, 7306-7311, doi:10.1073/pnas.1214441110.
42. Nikolic, J.; Belot, L.; Raux, H.; Legrand, P.; Gaudin, Y.; A, A.A. Structural basis for the recognition of LDL-receptor family members by VSV glycoprotein. *Nat Commun* **2018**, *9*, 1029, doi:10.1038/s41467-018-03432-4.
43. White, J.M.; Whittaker, G.R. Fusion of Enveloped Viruses in Endosomes. *Traffic* **2016**, *17*, 593-614, doi:10.1111/tra.12389.
44. Ono, N.; Tatsuo, H.; Hidaka, Y.; Aoki, T.; Minagawa, H.; Yanagi, Y. Measles viruses on throat swabs from measles patients use signaling lymphocytic activation molecule (CDw150) but not CD46 as a cellular receptor. *J Virol* **2001**, *75*, 4399-4401, doi:10.1128/JVI.75.9.4399-4401.2001.
45. Buchholz, U.J.; Finke, S.; Conzelmann, K.K. Generation of bovine respiratory syncytial virus (BRSV) from cDNA: BRSV NS2 is not essential for virus replication in tissue culture, and the human RSV leader region acts as a functional BRSV genome promoter. *J Virol* **1999**, *73*, 251-259.
46. Acciani, M.; Alston, J.T.; Zhao, G.; Reynolds, H.; Ali, A.M.; Xu, B.; Brindley, M.A. Mutational Analysis of Lassa Virus Glycoprotein Highlights Regions Required for Alpha-Dystroglycan Utilization. *J Virol* **2017**, *91*, doi:10.1128/JVI.00574-17.
47. Acciani, M.D.; Lay-Mendoza, M.F.; Havranek, K.E.; Duncan, A.M.; Iyer, H.; Linn, O.L.; Brindley, M.A. Ebola virus requires phosphatidylserine scrambling activity for efficient budding and optimal infectivity. *bioRxiv* **2020**, 10.1101/2020.03.16.994012, 2020.2003.2016.994012, doi:10.1101/2020.03.16.994012.
48. Salvador, B.; Zhou, Y.; Michault, A.; Muench, M.O.; Simmons, G. Characterization of Chikungunya pseudotyped viruses: Identification of refractory cell lines and demonstration of cellular tropism differences mediated by mutations in E1 glycoprotein. *Virology* **2009**, *393*, 33-41, doi:10.1016/j.virol.2009.07.013.

49. Zhao, P.; Praissman, J.L.; Grant, O.C.; Cai, Y.; Xiao, T.; Rosenbalm, K.E.; Aoki, K.; Kellman, B.P.; Bridger, R.; Barouch, D.H., et al. Virus-Receptor Interactions of Glycosylated SARS-CoV-2 Spike and Human ACE2 Receptor. *Cell Host Microbe* **2020**, *28*, 586-601 e586, doi:10.1016/j.chom.2020.08.004.
50. Ramakrishnan, M.A. Determination of 50% endpoint titer using a simple formula. *World J Virol* **2016**, *5*, 85-86, doi:10.5501/wjv.v5.i2.85.
51. Willard, K.A.; Elling, C.L.; Stice, S.L.; Brindley, M.A. The Oxysterol 7-Ketocholesterol Reduces Zika Virus Titers in Vero Cells and Human Neurons. *Viruses* **2018**, *11*, doi:10.3390/v11010020.
52. Li, W.; Moore, M.J.; Vasilieva, N.; Sui, J.; Wong, S.K.; Berne, M.A.; Somasundaran, M.; Sullivan, J.L.; Luzuriaga, K.; Greenough, T.C., et al. Angiotensin-converting enzyme 2 is a functional receptor for the SARS coronavirus. *Nature* **2003**, *426*, 450-454, doi:10.1038/nature02145.
53. Brecher, M.; Schornberg, K.L.; Delos, S.E.; Fusco, M.L.; Saphire, E.O.; White, J.M. Cathepsin cleavage potentiates the Ebola virus glycoprotein to undergo a subsequent fusion-relevant conformational change. *J Virol* **2012**, *86*, 364-372, doi:10.1128/JVI.05708-11.
54. Johannsdottir, H.K.; Mancini, R.; Kartenbeck, J.; Amato, L.; Helenius, A. Host cell factors and functions involved in vesicular stomatitis virus entry. *J Virol* **2009**, *83*, 440-453, doi:10.1128/JVI.01864-08.
55. Kim, I.S.; Jenni, S.; Stanifer, M.L.; Roth, E.; Whelan, S.P.; van Oijen, A.M.; Harrison, S.C. Mechanism of membrane fusion induced by vesicular stomatitis virus G protein. *Proc Natl Acad Sci U S A* **2017**, *114*, E28-E36, doi:10.1073/pnas.1618883114.
56. Wahlberg, J.M.; Boere, W.A.; Garoff, H. The heterodimeric association between the membrane proteins of Semliki Forest virus changes its sensitivity to low pH during virus maturation. *J Virol* **1989**, *63*, 4991-4997, doi:10.1128/JVI.63.12.4991-4997.1989.
57. Schornberg, K.; Matsuyama, S.; Kabsch, K.; Delos, S.; Bouton, A.; White, J. Role of endosomal cathepsins in entry mediated by the Ebola virus glycoprotein. *J Virol* **2006**, *80*, 4174-4178, doi:10.1128/JVI.80.8.4174-4178.2006.
58. Millet, J.K.; Tang, T.; Nathan, L.; Jaimes, J.A.; Hsu, H.L.; Daniel, S.; Whittaker, G.R. Production of Pseudotyped Particles to Study Highly Pathogenic Coronaviruses in a Biosafety Level 2 Setting. *J Vis Exp* **2019**, 10.3791/59010, doi:10.3791/59010.
59. Tani, H.; Morikawa, S.; Matsuura, Y. Development and Applications of VSV Vectors Based on Cell Tropism. *Front Microbiol* **2011**, *2*, 272, doi:10.3389/fmicb.2011.00272.
60. Whitt, M.A. Generation of VSV pseudotypes using recombinant DeltaG-VSV for studies on virus entry, identification of entry inhibitors, and immune responses to vaccines. *J Virol Methods* **2010**, *169*, 365-374, doi:10.1016/j.jviromet.2010.08.006.
61. Herder, M.; Graham, J.E.; Gold, R. From discovery to delivery: public sector development of the rVSV-ZEBOV Ebola vaccine. *Journal of Law and the Biosciences* **2020**, 10.1093/jlb/lsz019, doi:10.1093/jlb/lsz019.
62. Matz, K.M.; Marzi, A.; Feldmann, H. Ebola vaccine trials: progress in vaccine safety and immunogenicity. *Expert Rev Vaccines* **2019**, *18*, 1229-1242, doi:10.1080/14760584.2019.1698952.
63. Feneant, L.; Szymanska-de Wijs, K.M.; Nelson, E.A.; White, J.M. An exploration of conditions proposed to trigger the Ebola virus glycoprotein for fusion. *PLoS One* **2019**, *14*, e0219312, doi:10.1371/journal.pone.0219312.